THE JOURNAL OF COMPARATIVE NEUROLOGY 456:396–407 (2003)

Distribution of α-Amino-3-Hydroxy-5-Methyl-4-Isoxazolepropionate-Type Glutamate Receptor Subunits (GluR2/3) along the Ventral Visual Pathway in the Monkey

LIHUA XU,[1] HISASHI TANIGAWA,[2] AND ICHIRO FUJITA[1–3]*
[1]Core Research for Evolutional Science and Technology, Japan Science and Technology Corporation, Osaka 565-0871, Japan
[2]Department of Cognitive Neuroscience, Osaka University Medical School, Osaka 565-0871, Japan
[3]Graduate School of Frontier Biosciences and Graduate School of Engineering Science, Osaka University, Osaka 560-8531, Japan

ABSTRACT

By using immunohistochemical methods, we examined the distribution of cells expressing subunits of α-amino-3-hydroxy-5-methyl-4-isoxazolepropionate (AMPA)-selective glutamate receptors (GluR2/3) in the cortical areas of the occipitotemporal pathway in monkeys. GluR2/3-immunoreactive (-ir) cells were primarily pyramidal cells; this category, however, also included large stellate cells in layer IVB of the striate cortex (V1) and fusiform cells in layer VI of all the areas examined. GluR2/3 immunoreactivity differed among the areas in laminar distribution and intensity. In V1, GluR2/3-ir cells were identified mainly in layers II, III, IVB, and VI. The prestriate areas V2 and V4 and the inferior temporal areas TEO and TE contained GluR2/3-ir cells in layers II, III, and VI. In the TE, GluR2/3-ir cells were also abundant in layer V. In area 36 of the perirhinal cortex, neurons in layers II, III, V, and VI were labeled in a similar manner to the TE labeling, but with greater staining intensity and numbers, especially in layer V. Thus, GluR2/3 immunoreactivity increased rostrally along the pathway. Within V1 and V2, cells strongly stained for GluR2/3 formed clusters that colocalized with cytochrome oxidase (CO)-rich regions. These distinct laminar and regional distribution patterns of GluR2/3 expression may contribute to the specific physiological properties of neurons within various visual areas and compartments. J. Comp. Neurol. 456:396–407, 2003.

Indexing terms: inferior temporal cortex; primary visual cortex; glutamate receptor; cytochrome oxidase; monkey; immunohistochemistry

The occipitotemporal or "ventral" visual pathway of the monkey cerebral cortex, essential for object recognition (Mishkin et al., 1983), contains the hierarchically organized areas of the primary visual cortex (V1), prestriate areas V2 and V4, and areas TEO and TE within the inferior temporal cortex. These areas are defined by their visuotopographic representation and the afferent/efferent connections made with other cortical and subcortical structures (Felleman and Van Essen, 1991). The first two areas can also be subdivided into compartments by histochemical cytochrome oxidase (CO) reactivity. V1 is compartmentalized into CO-rich "blobs" and CO-poor "interblobs," whereas V2 is divided into CO-rich "thick" and "thin" stripes and CO-poor "pale" stripes (Horton and Hubel, 1981; Livingstone and Hubel, 1982; Tootell et al., 1983). Each area or compartment contains a unique pro-

*Correspondence to: Ichiro Fujita, Graduate School of Frontier Biosciences, Osaka University, Machikaneyama 1-3, Toyonaka, Osaka 560-8531, Japan. E-mail: fujita@fbs.osaka-u.ac.jp

Received 6 August 2002; Accepted 1 November 2002

DOI 10.1002/cne.10538

Published online the week of January 6, 2003 in Wiley InterScience (www.interscience.wiley.com).

file of neurons with distinct visual response properties (Hubel and Livingstone, 1987; DeYoe and Van Essen, 1988; Zeki and Shipp, 1988). Along the V1-to-TE pathway, the neuron's receptive field size increases, in conjunction with increases in the complexity of the stimulus configuration required for full neuronal activation (Gross et al., 1972; Desimone and Gross, 1979; Gattass et al., 1981, 1988; Tanaka et al., 1991; Gallant et al., 1993; Pasupathy and Connor, 1999; Hegdé and Van Essen, 2000). A recent study also demonstrates that the susceptibility to synaptic plasticity differs between V1 and TE, suggesting that modifiability of the neuronal circuit may also differ between the cortical areas (Murayama et al., 1997).

Anatomical aspects also differ between areas and compartments along the pathway; the tangential spread and morphological complexity of the basal dendrites of pyramidal neurons in layers III and V increase as successively more anterior areas of this pathway are considered (Lund et al., 1993; Elston and Rosa, 1998, 2000). In addition, V1 neurons within CO-rich blobs have larger dendritic fields than those in interblobs (Elston and Rosa, 1998). The size, center-to-center spacing, and spread of terminal arbors of intrinsic horizontal axons increase from caudal to rostral areas (Yoshioka et al., 1992; Amir et al., 1993; Lund et al., 1993; Fujita and Fujita, 1996). These morphological characteristics may allow the neurons of later stages in the pathway to integrate information from larger visual fields and larger populations of afferent neurons, allowing a more global level of visual processing (Amir et al., 1993; Elston and Rosa, 1998, 2000). Similarly, there exist rostrocaudal neurochemical gradients along the pathway. The concentration of an opiate receptor subtype (μ-like; Lewis et al., 1981), the phosphorylation of protein kinase C substrates (Nelson et al., 1987), and the numbers of calbindin-immunoreactive (-ir) pyramidal cells (Kondo et al., 1994) gradually increase toward the anterior portion of the ventral visual pathway. CO-rich regions also differ in a chemical manner from CO-poor compartments. In V1, strong calbindin D-28K immunoreactivity is distributed in CO-poor regions and layers (Celio et al., 1986). In contrast to the previous extensive physiological characterizations of the monkey visual cortex, however, a comprehensive molecular characterization of the occipitotemporal visual pathway has not been performed.

L-glutamate, the predominant excitatory neurotransmitter of the brain, exerts its function through glutamate receptors (GluRs; Fagg and Foster, 1983; Fonnum, 1984; Tsumoto, 1990). GluRs are grouped into subtypes by their molecular structure and signal transduction mechanism (Monaghan et al., 1989; Nakanishi, 1992). Ligand-gated ionotropic GluRs, oligomers of various subunits forming cation-selective channels, are classified into three subtypes, α-amino-3-hydroxy-5-methyl-4-isoxazolepropionate (AMPA)-type (GluR1–4), kainate-type (GluR5–7, KA1, KA2), and *N*-methyl-D-aspartate (NMDA)-type (NMDAR1, NMDAR2A–D) receptors. Metabotropic glutamate receptors are coupled to G-proteins to modulate intracellular messengers. Among these subtypes, AMPA-type and kainate-type GluRs primarily mediate fast synaptic excitatory neurotransmission. To characterize the neurochemical nature of the monkey visual cortex, we examined the distribution of various L-glutamate receptor subtypes along the ventral visual pathway using immunohistochemistry. We report the cellular pattern of immunoreactivity to an antibody recognizing the GluR2 and GluR3 subunits (GluR2/3) of AMPA-type GluRs. Preliminary results have been reported elsewhere (Xu et al., 1997).

MATERIALS AND METHODS

Ten young adult monkeys (nine *Macaca fuscata* and one *Macaca fascicularis*, body weight 4.2–6.5 kg) were utilized for analysis. One hemisphere from each animal was used for these studies, and the other hemisphere was used for additional experiments (Tanigawa and Fujita, 1997; Tanigawa et al., 1998a,b; Wang et al., 1998). All animal care and experimental procedures, in accordance with the NIH *Guide for the Care and Use of Laboratory Animals* (1996), were approved by the animal experiment committee of Osaka University.

Tissue preparation

Animals were sedated with ketamine hydrochloride (2.4–3.8 mg/kg, i.m.) and then anesthetized with an overdose (60 mg/kg, i.v.) of sodium pentobarbital. After injection of 1,000 IU heparin into the exposed heart, the descending aorta was clamped. Monkeys were perfused transcardially with 1 liter 0.1 M phosphate-buffered saline (PBS; pH 7.4), followed by 2 liters of a mixture of 4% paraformaldehyde, 0.2% picric acid, 0.1% glutaraldehyde in 0.1 M phosphate buffer (PB; pH 7.4) and then by 2 liters 4% paraformaldehyde in 0.1 M PB for 30–40 minutes. In two cases, the fixative contained 4% paraformaldehyde only. No differences in staining patterns were observed using the two perfusion protocols. After perfusion, the brains were removed from the skull, photographed, cut into blocks, postfixed in 4% paraformaldehyde fixative for 3–4 hours at 4°C, and immersed in a graded series (10%, 20%, 30%) of sucrose solutions in PB to facilitate cryoprotection and clearance of fixatives. All brains were then cut at 40 μm on a freezing microtome. To facilitate a comparison of the different cortical areas, six hemispheres were cut in a plane parallel to the superior temporal sulcus, such that a single section included both all major neocortical areas within the ventral pathway (i.e., V1, V2, V4, TEO, and TE) and the medial limbic structures, such as the perirhinal (PR) and entorhinal cortices (EC) and the hippocampal formation (Fig. 1). Coronal sections through the medial temporal lobe were made through two hemispheres to obtain a better view of the border between TE and PR. The opercular surface of V1 from the two remaining monkeys was flattened by pressing the samples against aluminum foil-covered dry ice. Tangential sections through V1 were prepared to analyze the relation of GluR2/3 immunoreactivity with CO-rich blobs.

Histological procedures

All sections were kept in serial order in 0.1 M PBS (pH 7.4). Every twelfth section (i.e., 480 μm interval) makes up a series; adjacent series of sections were separately processed for GluR2/3 immunohistochemistry, Nissl staining with cresyl violet, and CO histochemistry (Wong-Riley, 1979). The remaining sections were processed for immunohistochemical reactions for other GluRs and additional markers for parallel studies, including parvalbumin and γ-aminobutyric acid (GABA). For GluR2/3 immunohistochemistry, floating sections were incubated first in 0.3% H_2O_2 in 0.1 M PBS for 20 minutes to block endogenous peroxidase activity, then in 5% normal goat serum (NGS)

with 5% bovine serum albumin (BSA; Sigma, St. Louis, MO) in 0.1 M PBS for 1 hour at room temperature to block nonspecific binding. A commercially available rabbit antiserum (Upstate Biotechnology Inc., Lake Placid, NY) specific for a 21-residue synthetic peptide (KQNFATYKEGYNVYGIESVKI) corresponding to the C-terminus of rat GluR2 (with the additional of lysine at the N-terminus) was used as a primary antibody. This polyclonal antibody recognizes both the GluR2 and the GluR3 subunits (Craig et al., 1993; Martin et al., 1993a,b). Sections were incubated in diluted anti-GluR2/3 antiserum (0.5 μg/ml diluted in 0.1 M PBS containing 3% NGS and 2% BSA) with gentle agitation for 36–48 hours at 4°C. After three washes in PBS, sections were incubated for 2–3 hours in secondary antibody [biotinylated goat anti-rabbit IgG (H + L); Vector Laboratories, Burlingame, CA] diluted 1:200 in 0.1 M PBS containing 3% NGS and 2% BSA at room temperature. After rinsing with PBS, sections were processed for 1 hour with the avidin-biotin-peroxidase method using an ABC standard kit (Vector Laboratories). The peroxidase reaction product was visualized by incubation in 0.05% 3,3′-diaminobenzidine tetrahydrochloride (DAB; Sigma) with 0.01% H_2O_2 in 0.1 M PBS. The sections were then mounted on gelatin-coated slides, air dried, cleared in Hemo-De (Fischer Scientific, Chicago, IL), and coverslipped in Entellan (Merck, Darmstadt, Germany). The reaction products of a population of sections were intensified by adding 0.02% ammonium nickel sulfate to the DAB solution. As a control, the primary antibody was omitted from the reaction solution for a few sections per animal; no immunoreactive signal was produced under these circumstances.

All sections were examined under a light microscope (Eclipse E800; Nikon, Tokyo, Japan) equipped with bright-field illumination. Section images were captured digitally at 4× or 10× magnification using a 3CCD color video camera (DXC-950; Sony, Tokyo, Japan). Images of sections captured at high magnification were assembled into montages by using an image-analysis system (MCID; Imaging Research).

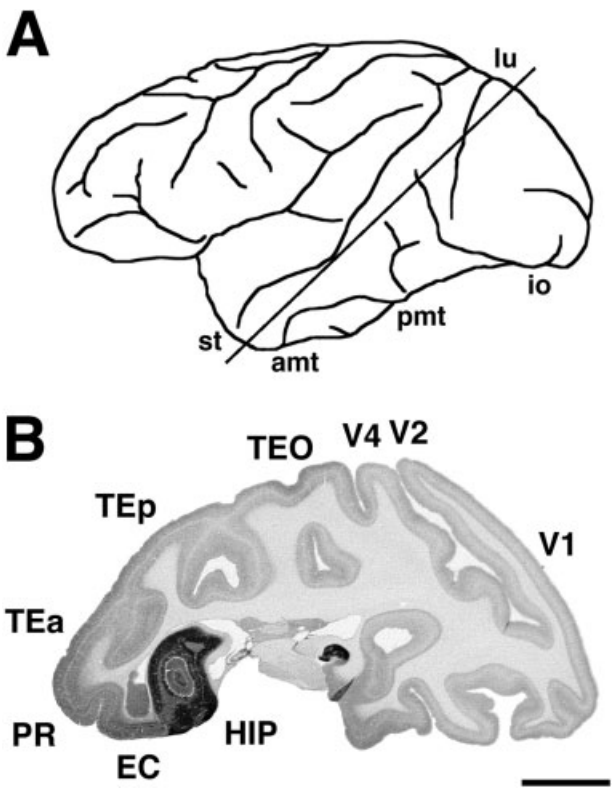

Fig. 1. Overall distribution of GluR2/3 immunoreactivity along the ventral visual pathway and in the medial limbic structures. **A:** Lateral view of a macaque left cerebral cortex. **B:** GluR2/3-immunostained section taken at the plane indicated by a straight line in A. The staining intensity exhibits an anteroposterior gradient. amt, Anterior middle temporal sulcus; io, inferior occipital sulcus; lu, lunate sulcus; pmt, posterior middle temporal sulcus; st, superior temporal sulcus; EC, entorhinal cortex; HIP, hippocampus; PR, perirhinal cortex; TEa, TEp, TEO, anterior and posterior parts of area TE and area TEO of the inferior temporal cortex; V1, V2, V4, visual cortical areas V1, V2, and V4. Scale bar = 10 mm.

RESULTS

The distribution pattern of GluR2/3 immunoreactivity was similar in both *M. fuscata* and *M. fascicularis*. The results obtained for the two species will be described together. All the figures contain results obtained using materials from *M. fuscata*.

Overall staining pattern

The overall distribution of GluR2/3 expression along the ventral visual pathway and in the medial temporal lobe can be observed in a single section, parallel to the superior temporal sulcus and cutting through the occipital and temporal cortices (Fig. 1). In these sections, the entire structure of the hippocampus was stained intensely. The gray matter of the neocortical and rhinal cortical areas was also immunoreactive for GluR2/3, at weaker levels than those seen for the hippocampus. Within the neocortical and rhinal cortical areas, the EC was most densely stained, followed by the PR, which was in turn stained more densely than the lateral and posterior neocortical regions, including the anterior and posterior TE, TEO, and V4–V1. This increase in GluR2/3 immunoreactivity observed toward the anterior part of the brain was consistent throughout all animals examined (n = 6). In the neocortical areas, staining in the middle layer was weaker than in the upper and lower layers; the middle portion of the gray matter appeared as a light band. This weakly immunoreactive band was either a part (in area V1) or the whole of layer IV (in the other cortices: V2, V4, TEO, TE) and layer V (in V2–TEO, but not in TE and PR; see below). This study focuses on areas of the ventral visual pathway (V1–V4, TEO, TE) and area 36 of the PR, to which TE projects.

Cellular localization

GluR2/3 was expressed primarily in neuronal somata, the proximal portion of the dendrites, and to a less extent neuropil. Most GluR2/3-ir neurons were identified as pyramidal cells from their somatic and dendritic morphology (Figs. 2A, 7). Labeled pyramidal cells differed in size between the layers and areas, exhibiting light, moderate, or strong GluR2/3 immunoreactivity. In layer IVB of V1, large, stellate cells were intensively immunoreactive for GluR2/3 (Fig. 2B). In layer VI throughout the regions examined, the irregularly shaped GluR2/3-ir cells were identified as asymmetric pyramidal or fusiform cells (Fig. 2C). The predominant cellular localization of GluR2/3 immunoreactivity to pyramidal cells was consistent with

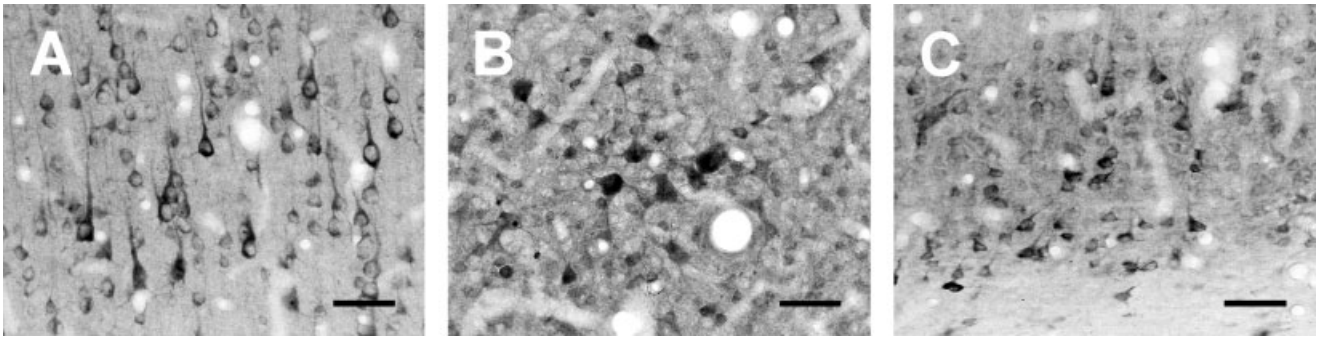

Fig. 2. Cellular localization of GluR2/3 immunoreactivity. **A:** GluR2/3-ir pyramidal cells with intensely stained somata and proximal dendrites regions in layer III of V4. **B:** GluR2/3-ir large stellate cells in layer IVB of V1. **C:** GluR2/3-ir fusiform and pyramidal cells in layer VI of V1. Scale bars = 50 μm.

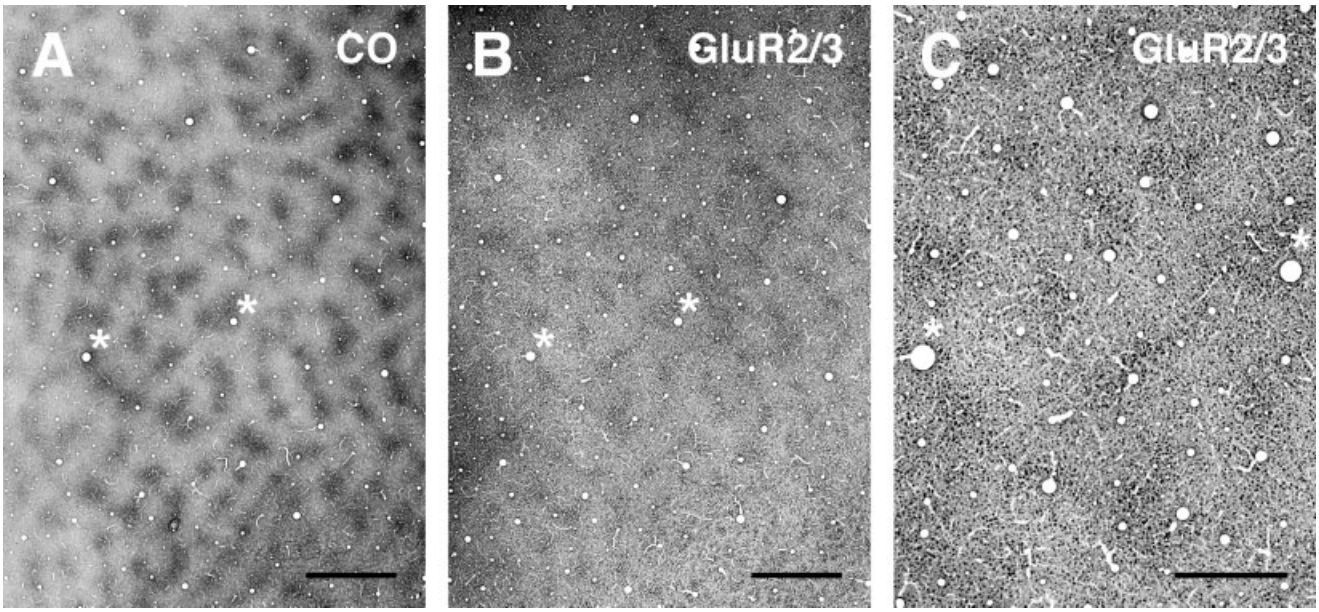

Fig. 3. Blob-like distribution pattern of GluR2/3 immunoreactivity in layer III of V1. A,B: A pair of adjacent tangential sections through layer III of V1, stained with either CO (**A**) or anti-GluR2/3 antiserum (**B**). GluR2/3 immunoreactivity was not evenly distributed throughout this layer; strongly labeled cells formed clusters. These clusters were in register with CO blobs in the adjacent section. **C:** High-magnification microphotograph from B. GluR2/3-ir clusters contained intensely stained GluR2/3-ir cells. Neuropil exhibited stronger staining than interblob regions. Asterisks indicate the corresponding radial blood vessels in each of the sections. Scale bars = 500 μm.

previous studies using similar antibodies in rats, cats, monkeys, and humans (Martin et al., 1993a,b; Vickers et al., 1993; Gutierrez-Igarza et al., 1996; Kohama and Urbanski, 1997; González-Albo et al., 2001), although the identification of neurons by morphological type is not completely reliable in immunohistochemical materials. In fact, a small population of GABAergic interneurons expresses GluR2/3 in the monkey prefrontal cortex (Vickers et al., 1993) and the human temporal lobe (Brodmann's area 21; González-Albo et al., 2001).

Regional distribution

Primary visual cortex (area V1). GluR2/3 immunoreactivity in layers II and III of V1 was not uniform in a tangential direction; strongly labeled neurons formed clusters. GluR2/3-ir cell clusters of similar size and configuration were distributed regularly with a center-to-center interval of approximately 500 μm in a tangential direction. We identified this structure in a pair of adjacent tangential sections through layer III by processing with CO histochemistry (Fig. 3A) and GluR2/3 immunohistochemistry (Fig. 3B). The strongly GluR2/3-ir neuron clusters were distributed in register with CO-rich blobs. The staining intensity of neuropil was also stronger within the clusters than in the external regions (Fig. 3C). Although CO-rich blobs were identified in both layers II and III (Fig. 4A), GluR2/3-ir cell clusters were also located in layers II and III, but centered on layer III (Figs. 4B, 7A). Both inside and outside the clusters of strongly GluR2/3-ir cells, lightly stained neurons existed in layers II and III. Most of these cells were recognizable as pyramidal cells from the morphology of the soma and apical dendrites.

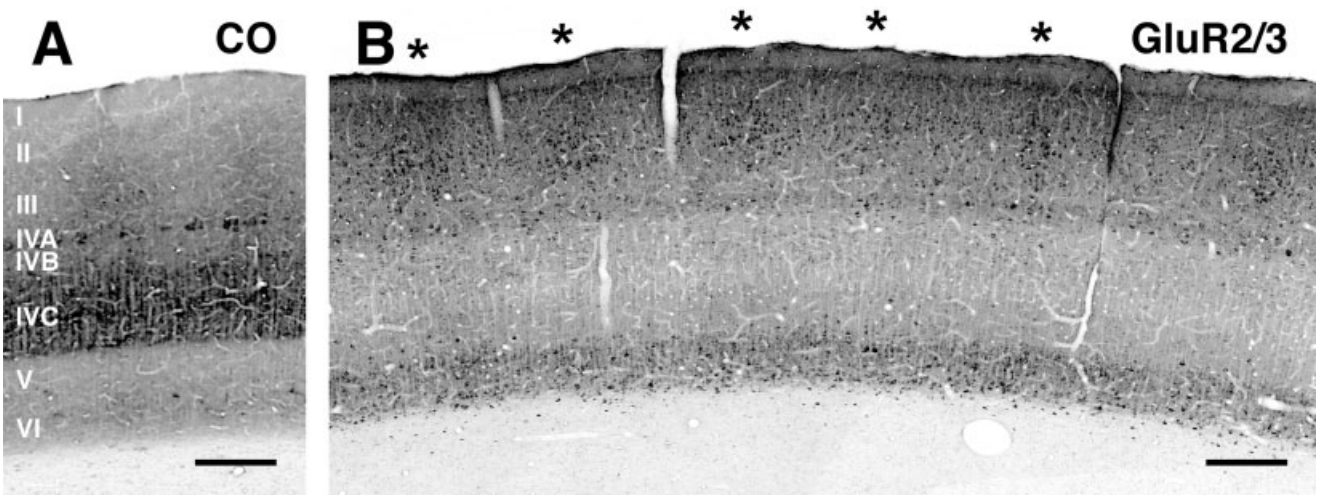

Fig. 4. Laminar distribution of GluR2/3 expression in V1. A and B are adjacent sections cut perpendicular to the pial surface. **A:** CO stained section. **B:** GluR2/3-immunostained section. Clusters of GluR2/3-ir pyramidal cells (asterisks) are regularly distributed throughout layers II and III. Upper layer II, layer IVB, and layer VI also demonstrated strong immunoreactivity for GluR2/3. GluR2/3-ir cells in layer IVB and layer VI also formed weak clusters. Scale bars = 200 μm.

In transverse sections, three densely stained laminar bands were observed at the upper, middle, and bottom parts of the gray matter, corresponding to upper layer II, layer IVB, and layer VI, respectively (Fig. 4). The upper band, residing at the junction of layers I and II, consisted of moderately stained, densely packed, small cells. These cells were round, without observable dendrites. The densely stained band in layer IVB consisted of both moderately stained pyramidal cells and darkly stained, large stellate cells. Tangential sections through this layer demonstrated that these stellate cells also formed clusters (Fig. 2B). Within a 40-μm-thick section, each cluster contained three to eight stellate cells. The layer VI band, containing moderately to strongly stained pyramidal cells, was characterized by heterogeneous darkly stained cells ranging in morphology from vertical and horizontal fusiform cells to smaller, asymmetric pyramidal cells (Fig. 2C). These three regions, upper layer II, layer IVB, and layer VI, also exhibited strong neuropil staining. In contrast, layers IVA, IVC, and V contained few GluR2/3-ir neurons, with weaker neuropil staining than was seen in the other layers.

Area V2. At the border between V1 and V2, the sudden appearance of large and heavily GluR2/3-ir pyramidal cells in layer III and the lack of GluR2/3 labeling in layer IV in V2 demarcated the two areas sharply (Fig. 5). The cells and neuropil of layer VI were stained moderately, whereas only small numbers of cells were even lightly stained in layer V. Layers I and IV were devoid of labeled neurons, with a light neuropil staining (Figs. 6B, 7B). As in V1, GluR2/3-ir V2 neurons in layers II and III were not evenly distributed along a tangential direction; strongly labeled regions alternated with lightly labeled ones. The strongly stained regions contained clusters of large, darkly labeled GluR2/3-ir cells (Fig. 6B). These clusters extended from layer II through layer III. Large pyramidal cells within the lower part of layer III were stained most intensely. The tangential extent of each cluster in V2, unlike that of V1, was variable (from 200 μm to 1 mm). Some clusters were close to each other, whereas others were farther apart. Beneath the strongly labeled regions of layers II and III, GluR2/3 immunoreactivity in layer VI was also slightly stronger than in the neighboring regions. When we examined immediately adjacent sections for CO staining, the GluR2/3-ir cell clusters in layers II and III in V2 were also in register with corresponding CO-rich regions (Fig. 6A,B) that represent the thick and thin CO-rich stripes (Tootell et al., 1983; Wong-Riley and Carroll, 1984). The correlation of GluR2/3-ir cell clusters and CO-rich thick and thin stripes was observed across consecutive sections in all animals.

Area V4 and inferior temporal cortex. The GluR2/3-ir cells in areas V4, TEO, and TE had a laminar distribution similar to that in V2, with the labeling of both supragranular and infragranular layers and the lack of labeled cells in layers I and IV (Fig. 7C–E). Positive cells were distributed evenly tangentially within the layers of these areas. No GluR2/3-ir cell clusters similar to those observed in areas V1 and V2 were identified. The lower tier of layer III stained most densely, containing large, darkly stained pyramidal cells with long apical dendrites. Layer II and the upper portion of layer III were moderately to strongly stained, possessing a greater density of smaller cells than the lower portion of layer III. Layer VI contained smaller immunoreactive cells, most of which were reduced in staining intensity from the layer II and III neurons. The three areas exhibited notable differences in labeling of layer V cells; V4 contained few labeled cells in layer V (Fig. 7C), whereas GluR2/3-ir layer V cells appeared in area TEO (Fig. 7D). This layer of area TE, however, contained many strongly GluR2/3-ir neurons (Fig. 7E).

The staining intensity of both the supragranular and the infragranular layers increased gradually from V1 through area TE. In a set of photographs taken of a single section and processed with identical imaging procedures, the intensity of staining in layer II/III increased from V 1 through TE (Fig. 7). Labeled layer V neurons appeared in

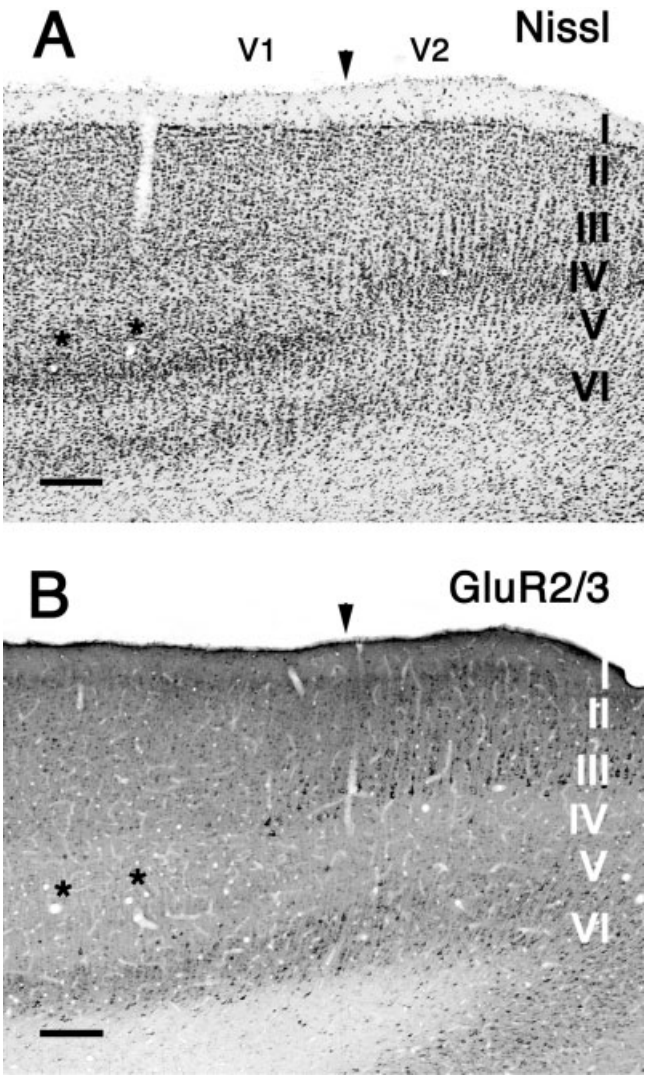

Fig. 5. Pattern of GluR2/3 expression at the boundary of V1 and V2. **A:** Section stained with cresyl violet. **B:** GluR2/3-immnostained section adjacent to the section showin in A. The appearance of a distinct population of GluR2/3-ir pyramidal neurons in layer III and the absence of staining in layer IV in area V2 sharply demarcate the border between V1 and V2. Arrowheads mark the position of the border. Asterisks indicate the same blood vessel in each of the two sections. Scale bars = 200 μm.

areas TEO and TE; their number and staining intensity increased further in area 36 of the PR. These changes occurred in a gradual fashion, with no sharp border present between neighboring areas, except at the borders of V1 and V2 (Fig. 5) and TE and PR (see below).

PR. The PR contains area 36 and area 35. Area 36 of the PR is located immediately medially to area TE. We distinguished, in Nissl-stained sections (Fig. 8B), area TE from area 36 of the PR by criteria similar to those of Suzuki and Amaral (1994a,b). Layers V and VI of area TE are separated, but this distinction is less clear in area 36. Layer II cells are smaller in area TE than in area 36, with the darkly stained layer II cells forming clumps in area 36 but not in area TE. In addition, the proportion of darkly stained large pyramidal cells in layer V is greater in area 36 than in TE. In Nissl-stained materials, however, these differences are often subtle and not easily discernible.

Whereas area 36 of the PR contained GluR2/3-ir cells in layers II, III, V, and VI, as in area TE (Fig. 7), two aspects of GluR2/3 immunoreactivity differentiated these areas. In TE, staining intensity of the supragranular layer was stronger than that of the infragranular layer, whereas the staining intensity of both somata and neuropil was comparable between the supragranular and infragranular layers in area 36 of the PR (Fig. 7E,F). In addition, GluR2/3 immunoreactivity in area 36 of the PR was marked by an increase in darkly stained large GluR2/3-ir neurons in layer V compared with those in TE, with both the supragranular and the infragranular layers appearing darker in the PR than in area TE (Fig. 8).

DISCUSSION

By using immunohistochemical methods, we localized cells and neuropil expressing GluR2/3 in visual cortical areas along the occipitotemporal pathway of the monkey. This study examined specific laminar, compartmental, and regional distribution patterns of GluR2/3-ir cells and neuropil. We identified differences in GluR2/3 immunoreactivity among the areas in laminar distribution and intensity, an anterior-posterior gradient of GluR2/3 immunoreactivity in the cortical areas, a differential distribution of GluR2/3 expression in CO-rich and CO-poor compartments in V1 and V2, and a clear border between area TE and area 36 of the PR defined by differences in GluR2/3 immunoreactivity.

Different distribution patterns of GluR2/3 immunoreactivity among ventral visual areas

In their examination of the distribution of various GluRs in the monkey medial temporal regions, Kohama and Urbanski (1997) reported that the distribution of GluR2/3 is more homogenous throughout the hippocampus, EC, temporal cortex, and basal ganglia areas than the distribution of GluR1. It can still be seen in their immunohistochemical images that GluR2/3 immunostaining is densest in the hippocampus, with moderate reactivity in the EC and PR and weaker staining in the temporal neocortex. By sectioning parallel to the superior temporal sulcus, we have extended our observations to earlier stages of the visual pathway. We identified a rostrocaudal gradient of GluR2/3 immunoreactivity throughout the neocortical areas in the ventral visual pathway. These changes in staining intensity do not result from simple differences in cell density among the different cortical areas nor sectioning artifacts, such as uneven thickness or reaction efficiency. In actuality, the cell density of V1 is twice that of the other areas (O'Kusky and Colonnier, 1982; Peters, 1987), despite stronger GluR2/3 immunoreactivity in the anterior areas. The staining patterns of additional antibodies, examined in adjacent sections from the same animal, showed distinct distribution patterns, demonstrating the specificity of GluR2/3 staining; parvalbumin immunoreactivity, for example, was highest in V1 and gradually decreased anteriorly along the ventral pathway, as has been previously reported (Kondo et al., 1994). In addition, the staining intensity in supragranular

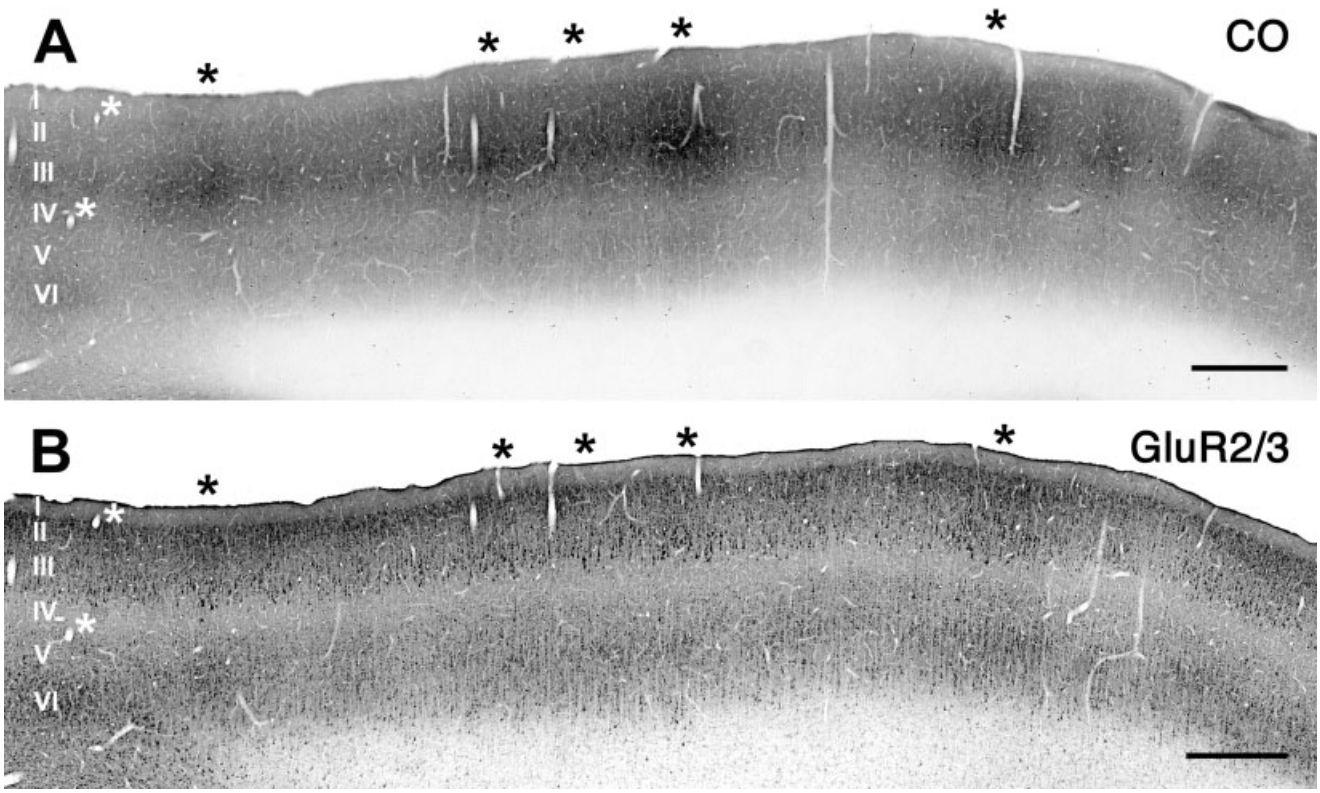

Fig. 6. Uneven distribution of GluR2/3 immunoreactivity in area V2. A and B are adjacent sections cut perpendicular to the pial surface. **A:** CO-stained section. **B:** GluR2/3-immunostained section. Strong GluR2/3 immunoreactivity was observed in layers II, III, and VI. In layer II/III, intensely immunoreactive regions alternated with lightly stained regions. The distance between these areas was irregular. A comparison of A and B indicates that intensely stained GluR2/3-ir regions corresponded to CO-rich regions. Black asterisks indicate the corresponding location of CO-rich and GluR2/3-immunoreactive regions. White asterisks indicate the corresponding blood vessels in each of the two sections. Scale bars = 500 μm.

and infragranular layers did not change in a parallel manner. The supragranular layer possessed a higher intensity of staining than the infragranular layer in areas V2 to TE, whereas, in the PR, the staining intensity in the supragranular and infragranular layers was comparable. These observations indicate that the pattern of staining reflects a gradient of GluR2/3 immunoreactivity throughout the occipitotemporal visual pathway.

GluR2/3 immunoreactivity demarcated the border between area V1 and V2. Because of the substantial differences in the V1 and V2 laminar structures, the V1/V2 border can easily be identified in Nissl- and CO-stained sections. There is also a difference in immunoreactivity to neurofilaments and parvalbumin between the two areas (Hof and Morrison, 1995; DeFelipe et al., 1999; Goodchild and Martin, 1998; our unpublished observations). GluR2/3 can thus be added to the list of neurochemicals possessing distinct laminar and cellular distributions throughout V1 and V2.

It should be pointed out here that we adopt the widely used nomenclature of V1 cortical layers proposed by Brodmann (1909) for macaque monkeys in order to follow the majority of reports on V1 and avoid confusion. However, layer IVA/B of Brodmann has been suggested to belong to subdivisions of layer III, insofar as it contains many pyramidal neurons projecting to target cortical areas in both the ipsilateral and the contralateral hemispheres (Casagrande and Kaas, 1994; Elston and Rosa, 1998). The present results showing that layers IVA and IVB, but not IVC, contained GluR2/3-ir neurons suggest that the distribution of GluR2/3-ir neurons in supragranular and granular layers would show a qualitatively similar pattern in all areas examined, if layer IVC was considered to be the "true" layer IV. The present results thus add support to the alternative nomenclature of the V1 layers (Hassler, 1966).

Area TE of the inferior temporal cortex of macaque monkeys, residing near the end of the ventral visual pathway, is critical for visual processing related to object recognition. Area TE provides a major input for the PR. The PR, part of the medial temporal lobe belonging to the

Fig. 7. Comparison of laminar and cellular localization of GluR2/3 expression among V1 (**A**), V2 (**B**), V4 (**C**), area TEO (**D**), area TE (**E**), and area 36 of the PR (**F**). Photographs were taken of various parts of a single section and processed with exactly identical imaging procedures. In all areas, layers II, III, and VI are labeled. Layer IV lacked staining in all areas except for V1. Layer V cells also stained positively for GluR2/3 within area TE and PR; PR demonstrates significantly stronger staining than TE. From V1 to TE, the staining intensity of the supragranular layers was of higher intensity than that of the infragranular layers, whereas in F the staining intensities of supragranular and infragranular layers are comparable. Scale bars = 200 μm.

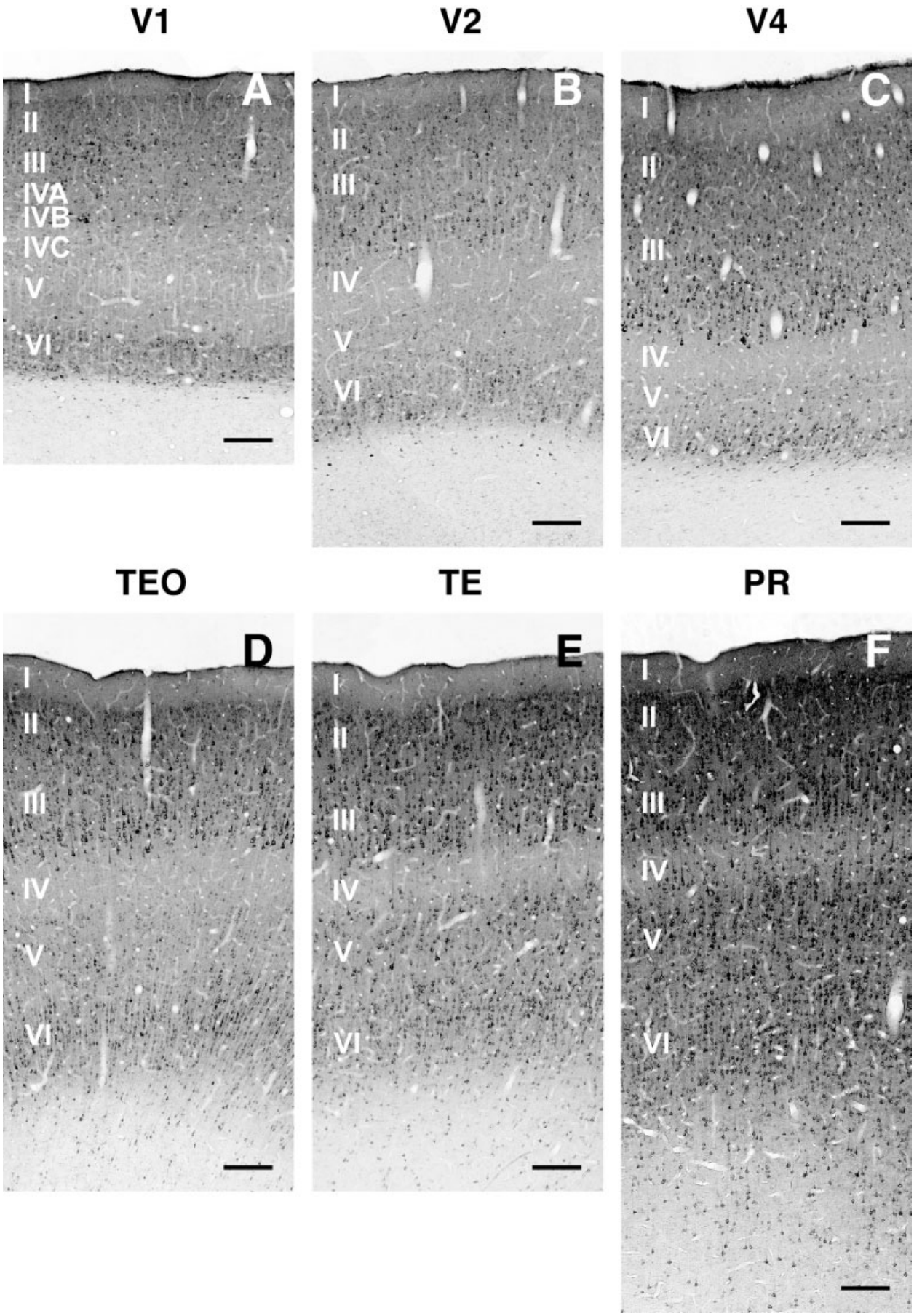

Figure 7

limbic system, is critically involved in visual recognition memory (Squire and Zola-Morgan, 1991; Miyashita, 1994; Suzuki, 1996). Difficulties in determining the exact border between the two areas have made interpretation of the results of some previous behavioral and anatomical studies unclear. Only recently have the differential contributions of area TE and the PR to visual perception and the formation of memory been experimentally demonstrated (Buffalo et al., 1999). Conflicting reports on the nature of the connection between the unimodal visual area TE and the hippocampus (Yukie and Iwai, 1988; Suzuki and Amaral, 1990) may result from discrepancies in the definitions of the border between area TE and the PR. In our sections, the PR was distinguished from TE by increased immunoreactivity in all the labeled layers, with a marked increase in the number of heavily stained, large layer V neurons. This characteristic makes it possible to distinguish the TE/PR border more clearly and may provide a valuable aid for the performance of consistent physiological, anatomical, and behavioral studies.

Regional specialization at cellular and molecular levels can provide a neurochemical basis for the distribution of visual function. GluR2/3-ir cells may be related to specific physiological attributes, such as synaptic plasticity (cf. Murayama et al., 1997). It is unlikely, however, that such properties can be specified by GluR2/3 expression alone. Additional neurochemicals have distinct distribution patterns throughout different cortical regions, including calbindin D-28 expressed in pyramidal cells (Kondo et al., 1994), and phosphorylation substrates of protein kinase C (Nelson et al., 1987). Metabolic GluR2/3-ir neuropil staining (Tanigawa et al., 1998a) also gradually increases from posterior to anterior areas.

Correlation with CO-rich compartments in V1 and V2

Many neurons within the CO-rich blobs of V1 tune to low spatial frequencies and exhibit poor orientation and good spectral sensitivities; those outside CO-rich blobs prefer high spatial frequencies and are selective to orientation but respond to a broadband spectrum (Livingstone and Hubel, 1984; Ts'o and Gilbert, 1988; Silverman et al., 1989; Born and Tootell, 1991). CO-rich thick and thin stripes and CO-poor (pale) stripes in V2, containing different proportions of cells with various visual response properties, receive distinct inputs from different layers or CO compartments in V1 (Tootell et al., 1983; DeYoe and Van Essen, 1985; Shipp and Zeki, 1985). In addition to these anatomical and physiological characteristics, the chemical nature of these regions, defined by CO histochemistry, also differs in both V1 and V2. In squirrel monkeys, a neurochemically specific subpopulation of calbindin D-28-expressing GABA neurons is distributed in a pattern similar to that of CO-rich blobs in layers II and III of V1 (Celio et al., 1986). The staining pattern of Cat-301, a monoclonal antibody recognizing subpopulations of pyramidal and nonpyramidal neurons, is in register with CO-rich blobs in V1 and CO-rich stripes in area V2 (Hendry et al., 1988; DeYoe et al., 1990). The colocalization of GluR2/3-ir pyramidal cell clusters in layers II and III with CO-rich compartments in V1 and V2 indicates that glutamatergic transmission mechanisms differ between CO-rich and CO-poor compartments in both V1 and V2. We did not observe heterogeneity in GluR2/3 immunoreactivity across the cortex in V4, TEO, and TE.

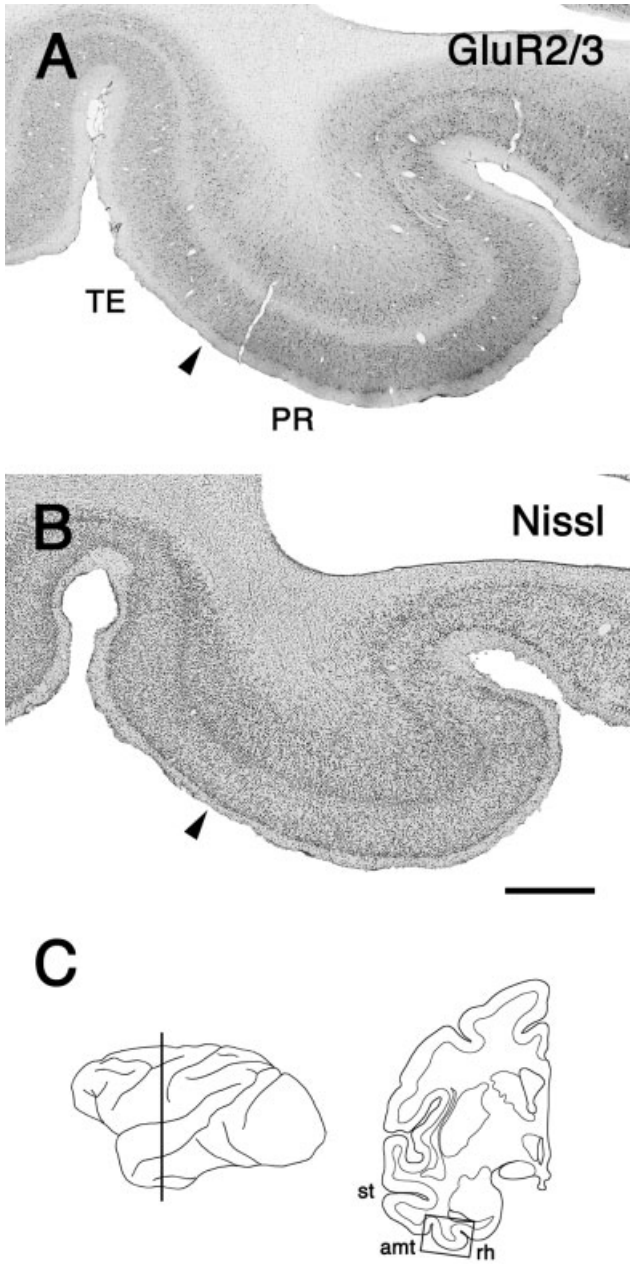

Fig. 8. GluR2/3 immunoreactivity in the ventral part of the inferior temporal cortex. GluR2/3-immunostained (**A**) and Nissl-stained (**B**) sections are demarcated by the rectangle in **C**. Arrowheads indicate the border between area TE and area 36 of the PR. The staining intensity of both supragranular and infragranular layers of the PR is stronger than that of TE. Note also the marked increase of darkly stained, large GluR2/3-ir neurons in layer V of area 36. rh, Rhinal sulcus. See Figure 1 legend for other abbreviations. Scale bar = 500 μm for A,B.

Our results differ from the report of Carder (1997) in both the cellular and the laminar localization of GluR2/3 expression. At the cellular level, GluR2/3 was observed in a predominant neuropil staining, whereas we discovered a major pyramidal somatic staining in all areas examined. The cellular location of GluR2/3 immunoreactivity in our

study, however, is in accordance with additional studies using similar antibodies in various animals (Martin et al., 1993a,b; Vickers et al., 1993; Ginsberg et al., 1995; Kohama and Urbanski, 1997). Carder (1997) reported dense staining in layers IVA, IVC, and VI within area V1 at the laminar distribution level, with modest staining in layers II/III, IVB, and V, suggesting that the layers innervated by afferents from the lateral geniculate nucleus are rich in GluR2/3. In the present study, however, layers II/III, IVB, and VI were stained intensely. In addition, layers IVA and IVC, the major geniculate recipient layers, were devoid of staining. Although we both observed a patch-like distribution of GluR2/3 immunoreactivity in layer II /III of area V1 coinciding with CO-rich blobs, the cellular observations differed greatly. We compared the experimental procedures in Carder's (1997) and our studies, but could not find any major methodological difference. Carder used *M. fascicularis*, and we used mostly *M. fuscata*. However, we confirmed that the two species exhibited identical staining patterns. The two studies used similar histological procedures and antibodies raised against the same peptide sequence (albeit from different companies, Chemicon in Carder's study and Upstate Biotechnology in ours). Thus, the explanation for the discrepancies remains unclear.

Functional implication of differential distribution of GluR2/3

Recent studies suggest that selective changes in expression of certain glutamate receptor subunits may contribute to the pathophysiological processes of brain disorders, such as ischemia, epilepsy, and neurodegenerative disease. Excessive receptor stimulation induces excitotoxic neuronal cell death, caused by abnormal influx of Ca^{2+} through glutamate receptors (Choi, 1988; McDonald, et al., 1998). GluR2 is suspected to serve as a "molecular switch" determining the permeability of Ca^{2+} through AMPA receptors (Boulter et al., 1990; Hollmann et al., 1991). Thus, GluR2 influences neuronal vulnerability to these pathogenic processes (Pellegrini-Giampietro et al., 1997). In transient forebrain ischemia induced in rats, GluR2 gene expression is reduced in CA1 area. In addition, mRNAs for the GluR2 and GluR3 subunits are downregulated in the CA3 and CA4 regions of the hippocampus of rats subjected to kainate-induced epileptogenesis (Pellegrini-Giampietro et al., 1992, 1997; Friedman et al., 1994). GluR2/3 immunoreactivity is also decreased in the EC of patients with Alzheimer's disease (Armstrong et al., 1994). The initial pathologic changes in Alzheimer's disease begin in the limbic system: Neurofibrillary tangles first appear in the EC and then progress to other limbic structures, finally spreading to neocortical areas in a cell- and layer-specific manner (Braak and Braak, 1991). Although the limbic system, including PR, EC, hippocampus, and amygdala, is highly susceptible to the development of temporal lobe epilepsy, the primary visual area is rarely affected (Schwabe et al., 2000; Stoop and Pralong., 2000). Higher levels of expression of GluR2/3 in the limbic system and the lowest level of expression in V1 may explain the different vulnerabilities of different cortical areas to epilepsy or Alzheimer's disease.

ACKNOWLEDGMENTS

We thank Kathleen S. Rockland for her comments on an earlier version of the manuscript, Kayoko Nakagawa for her help with histology, and Atushi Hayashi for kindly providing the brains of *Macaca fascicularis*. This work was supported by grants to I.F. from the Science and Technology Corporation of Japan (Core Research of Evolutionary Science and Technology), the Science and Technology Agency (Special Coordination Funds for Promoting Science and Technology), and the Ministry of Education, Science, Sports, and Culture of Japan.

LITERATURE CITED

Amir Y, Harel M, Malach R. 1993. Cortical hierarchy reflected in the organization of intrinsic connections in macaque monkey visual cortex. J Comp Neurol 334:19–46.

Armstrong DM, Ikonomovic MD, Sheffield R, Wenthold RJ. 1994. AMPA-selective glutamate receptor subtype immunoreactivity in the entorhinal cortex of non-demented elderly and patients with Alzheimer's disease. Brain Res 639:207–216.

Born RT, Tootel RB. 1991. Spatial frequency tuning of single units in macaque supragranular striate cortex. Proc Natl Acad Sci USA 88: 239–259.

Boulter J, Holmann M, O'Shea-Greenfield A, Hartley M, Deneris E, Maron C, Heinemann S. 1990. Molecular cloning and functional expression of glutamate receptor genes. Science 249:1033–1036.

Braak H, Braak E. 1991. Neuropathological staging of Alzheimer related neurofibrillary changes. Acta Neuropathol 82:239–259.

Brodmann K. 1909. Vergleichende Lokalisationslehre der Grosshirnrinde. Edited and translated by Garey JC. London: Smith-Gordon.

Buffalo EA, Ramus SJ, Clark RE, Teng E, Squire LR, Zola SM. 1999. Dissociation between the effects of damage to perirhinal cortex and area TE. Learn Mem 6:572–599.

Carder RK. 1997. Immunocytochemical characterization of AMPA-selective glutamate receptor subunits: laminar and compartmental distribution in macaque striate cortex. J Neurosci 17:3352–3363.

Casagrande VA, Kaas JH. 1994. The afferent, intrinsic and efferent connections of primary visual cortex in primates. In: Peters A, Rockland KS, editors. Cerebral cortex, vol 10: primary visual cortex in primates. New York: Plenum. p 201–259.

Celio MR, Scharer L, Morrison JH, Norman AW, Bloom FE. 1986. Calbindin immunoreactivity alternates with cytochrome *c*-oxidase-rich zones in some layers of the primate visual cortex. Nature 323:715–717.

Choi DW. 1988. Glutamate neurotoxicity and diseases of the nervous system. Neuron 1:623–634.

Craig AM, Blackstone CD, Huganir RL, Banker G. 1993. The distribution of glutamate receptors in cultured rat hippocampal neurons: postsynaptic clustering of AMPA-selective subunits. Neuron 10:1055–1068.

DeFelipe J, González-Albo MC, del Río MR, Elston GN. 1999. Distribution and patterns of connectivity of interneurons containing calbindin, calretinen and parvalbumin in visual areas of the occipital and temporal lobes of the macaque monkey. J Comp Neurol 412:515–526.

Desimone R, Gross CG. 1979. Visual areas in the temporal cortex of the macaque. Brain Res 178:363–380.

DeYoe EA, Van Essen DC. 1985. Segregation of efferent connections and receptive properties in visual area V2 of the macaque. Nature 317:58–61.

DeYoe EA, Van Essen DC. 1988. Concurrent processing streams in monkey visual cortex. Trends Neurosci 11:219–226.

DeYoe EA, Hockfield S, Garren H, Van Essen DC. 1990. Antibody labeling of functional subdivisions in visual cortex: Cat-301 immunoreactivity in striate and extrastriate cortex of the macaque monkey. Vis Neurosci 5:67–81.

Elston GN, Rosa MG. 1998. Morphological variation of layer III pyramidal neurones in the occipitotemporal pathway of the macaque monkey visual cortex. Cereb Cortex 8:278–294.

Elston GN, Rosa MG. 2000. Pyramidal cells, patches, and cortical columns: a comparative study of infragranular neurons in TEO, TE, and the superior temporal polysensory area of the macaque monkey. J Neurosci 20:RC117.

Fagg GE, Foster AC. 1983. Amino acid neurotranmitters and their pathways in the mammalian central nervous system. Neuroscience 9:701–719.

Felleman DJ, Van Essen DC. 1991. Distributed hierarchical processing in the primate cerebral cortex. Cereb Cortex 1:1–47.

Fonnum F. 1984. Glutamate: a neurotransmitter in mammalian brain. J Neurochem 42:1–11.

Friedman LK, Pellegrini-Giampietro DE, Sperber EF, Bennett MV, Moshe SL, Zukin RS. 1994. Kainate-induced status epilepticus alters glutamate and $GABA_A$ receptor gene expression in adult rat hippocampus: an in situ hybridization study. J Neurosci 14:2697–2707.

Fujita I, Fujita T. 1996. Intrinsic connections in the macaque inferior temporal cortex. J Comp Neurol 368:467–486.

Gallant JL, Braun J, Van Essen DC. 1993. Selectivity for polar, hyperbolic and Cartesian gratings in macaque visual cortex. Science 259:100–103.

Gattass R, Gross CG, Sandell JH. 1981. Visual topography of V2 in the macaque. J Comp Neurol 201:519–539.

Gattass R, Sousa APB, Gross CG. 1988. Visuotopic organization and extent of V3 and V4 of the macaque. J Neurosci 8:1831–1856.

Ginsberg SD, Price DL, Blackstone CD, Huganir RL, Martin LJ. 1995. Non-NMDA glutamate receptors are present throughout the primate hypothalamus. J Comp Neurol 353:539–552.

González-Albo MC, Elston GN, DeFelipe J. 2001. The human temporal cortex: characterization of neurons expressing nitric oxide synthase, neuropeptides and calcium-binding proteins, and their glutamate receptor subunit profiles. Cereb Cortex 11:1170–1181.

Goodchild AK, Martin PR. 1998. The distribution of calcium binding proteins in the lateral geniculate nucleus and visual cortex of a New World monkey, the marmoset, *Callithrix jacchus*. Vis Neurosci 15:625–642.

Gross CG, Rocha-Miranda CE, Bender DB. 1972. Visual properties of neurons in inferotemporal cortex of the macaque. J Neurophysiol 35: 96–111.

Gutierrez-Igarza K, Fogarty DJ, Perez-Cerda F, Donate-Oliver F, Albus K, Matute C. 1996. Localization of AMPA-selective glutamate receptor subunits in the adult cat visual cortex. Vis Neurosci 13:61–72.

Hassler R. 1966. Comparative anatomy of the central visual system in day- and night-active primates. In: Hassler R, Stephan H, editors. Evolution of the forebrain. Sttutgart: Thieme. p 419–434.

Hegdé J, Van Essen DC. 2000. Selectivity for complex shapes in primate visual area V2. J Neurosci RC61:1–6.

Hendry SHC, Jones EG, Hockfield S, McKay R. 1988. Neuronal populations stained with the monoclonal antibody, Cat-301, in the mammalian cerebral cortex and thalamus. J Neurosci 8:518–542.

Hof PR, Morrison JH. 1995. Neurofilament protein defines regional patterns of cortical organization in the macaque monkey visual system: a quantitative immunohistochemical analysis. J Comp Neurol 352:161–186.

Hollmann M, Hartley M, Heinemann S. 1991. Ca^{2+} permeability of KA-AMPA-gated glutamate receptor channels depends on subunit composition. Science 252:851–853.

Horton JC, Hubel DH. 1981. Regular patchy distribution of cytochrome oxidase staining in primary visual cortex of macaque monkey. Nature 292:762–764.

Hubel DH, Livingstone MS. 1987. Segregation of form, color, and stereopsis in primate area 18. J Neurosci 7:3378–3415.

Kohama SG, Urbanski HF. 1997. Distribution of glutamate receptor subunits in the primate temporal cortex and hippocampus. Brain Res 769:44–56.

Kondo H, Hashikawa T, Tanaka K, Jones EG. 1994. Neurochemical gradient along the monkey occipito-temporal cortical pathway. Neuroreport 5:613–616.

Lewis ME, Mishkin M, Bragin E, Brown RM, Pert CB, Pert A. 1981. Opiate receptor gradients in monkey cerebral cortex: correspondence with sensory processing hierarchies. Science 211:1166–1169.

Livingstone MS, Hubel DH. 1982. Thalamic inputs to cytochrome oxidase-rich regions in monkey visual cortex. Proc Natl Acad Sci USA 79:6098–6101.

Livingstone MS, Hubel DH. 1984. Anatomy and physiology of a color system in the primate visual cortex. J Neurosci 4:309–356.

Lund JS, Yoshioka T, Levitt JB. 1993. Comparison of intrinsic connectivity in different areas of macaque monkey cerebral cortex. Cereb Cortex 3:148–162.

Martin LJ, Blackstone CD, Levey AI, Huganir RL, Price DL. 1993a. Cellular localizations of AMPA glutamate receptors within the basal forebrain magnocellular complex of rat and monkey. J Neurosci 13:2249–2263.

Martin LJ, Blackstone CD, Levey AI, Huganir RL, Price DL. 1993b. AMPA glutamate receptor subunits are differentially distributed in rat brain. Neuroscience 53:327–358.

McDonald JW, Bhattacharyya T, Sensi SL, Lobner D, Ying HS, Canzoniero LM, Choi DW. 1998. Extracellular acidity potentiates AMPA receptor-mediated cortical neuronal death. J Neurosci 18:6290–6299.

Mishkin M, Ungerleider LG, Macko KA. 1983. Object vision and spatial vision: two cortical pathways. Trends Neurosci 6:414–417.

Miyashita Y. 1994. Inferior temporal cortex: where visual perception meets memory. Annu Rev Neurosci 16:245–263.

Monaghan DT, Bridges RJ, Cotman CW. 1989. The excitatory amino acid receptors: their class, pharmacology, and distinct properties in the function of the central nervous system. Annu Rev Pharmacol Toxicol 29:365–402.

Murayama Y, Fujita I, Kato M. 1997. Contrasting forms of synaptic plasticity in monkey inferotemporal and primary visual cortices. Neuroreport 8:1503–1508.

Nakanishi S. 1992. Molecular diversity of glutamate receptors and implications for brain function. Science 258:597–603.

Nelson RB, Friedman DP, O'Neill JB, Mishkin M, Routtenberg A. 1987. Gradients of protein kinase C substrate phosphorylation in primate visual system peak in visual memory storage areas. Brain Res 416: 387–392.

O'Kusky J, Colonnier M. 1982. A laminar analysis of the number of neurons, glia and synapses in the visual cortex (area 17) of adult macaque monkeys. J Comp Neurol 210:278–290.

Pasupathy A, Connor CE. 1999. Responses to contour features in macaque area V4. J Neurophysiol 82:2490–2502.

Pellegrini-Giamepietro DE, Zukin RS, Bennett MV, Cho S, Pulsinelli WA. 1992. Swich in glutamate receptor subunit gene expression in CA1 subfield of hippocampus following global ischemia in rats. Proc Natl Acad Sci USA 89:10499–10503.

Pellegrini-Giampietro DE, Gorter JA, Bennett MV, Zukin RS. 1997. The GluR2 (GluR-B) hypothesis: Ca^{2+}-permeable AMPA receptors in neurological disorders. Trends Neurosci 20:464–470.

Peters A. 1987. Number of neurons and synapses in primary visual cortex. In: Jones EG, Peters A, editors. Cerebral cortex, vol 6: further aspects of cortical function, including hippocampus. New York: Plenum. p 267–294.

Schwabe K, Ebert U, Loscher W. 2000. Effects of lesions of the perirhinal cortex on amygdala kindling in rats. Epilepsy Res 42:33–41.

Shipp S, Zeki S. 1985. Segregation of pathways leading from area V2 to areas V4 and V5 of macaque monkey visual cortex. Nature 315:322–325.

Silverman MS, Grosof DH, DeValois RL, Elfar SD. 1989. Spatial-frequency organization in primate striate cortex. Proc Natl Acad Sci USA 86:711–715.

Squire LR, Zola-Morgan S. 1991. The medial temporal lobe memory system. Science 253:1380–1386.

Stoop R, Pralong E. 2000. Functional connections and epileptic spread between hippocampus, entorhinal cortex and amygdala in a modified horizontal slice preparation of the rat brain. Eur J Neurosci 12:3651–3663.

Suzuki WA 1996. The anatomy, physiology and functions of the perirhinal cortex. Curr Opinion Neurobiol 6:179–186.

Suzuki WA, Amaral DG. 1990. Cortical inputs to the CA1 field of the monkey hippocampus originate from the perirhinal and parahippocampal cortex but not from area TE. Neurosci Lett 115:43–48.

Suzuki WA, Amaral DG. 1994a. Perirhinal and parahippocampal cortices of the macaque monkey: cortical afferents. J Comp Neurol 350:497–533.

Suzuki WA, Amaral DG. 1994b. Topographic organization of the reciprocal connections between the monkey entorhinal cortex and the perirhinal and parahippocampal cortices. J Neurosci 14:1856–1877.

Tanaka K, Saito H-A, Fukada Y, Moriya M. 1991. Coding visual images of objects in the inferotemporal cortex of the macaque monkey. J Neurophysiol 66:170–189.

Tanigawa H, Fujita I. 1997. Topographical relation between horizontal projections from adjacent sites in the macaque inferior temporal cortex: a double anterograde labeling study. Soc Neurosci Abstr 23:2062.

Tanigawa H, Xu LH, Fujita I. 1998a. Postnatal development of expression of mGluR2/3 and GluR2/3 in the primary visual cortex of the macaque monkey. Soc Neurosci Abstr 24:1877.

Tanigawa H, Fujita I, Kato M, Ojima H. 1998b. Distribution, morphology, and gamma-aminobutyric acid immunoreactivity of horizontally projecting neurons in the macaque inferior temporal cortex. J Comp Neurol 401:129–143.

Tootell RB, Silverman MS, De VR, Jacobs GH. 1983. Functional organization of the second cortical visual area in primates. Science 220:737–739.

Ts'o DY, Gilbert CD. 1988. The organization of chromatic and spatial interactions in the primate striate cortex. J Neurosci 8:1712–1727.

Tsumoto T. 1990. Excitatory amino acid transmitters and their receptors in neural circuits of the cerebral neocortex. Neurosci Res 9:79–102.

Vickers JC, Huntley GW, Edwards AM, Moran T, Rogers SW, Heinemann SF, Morrison JH. 1993. Quantitative localization of AMPA/kainate and kainate glutamate receptor subunit immunoreactivity in neurochemically identified subpopulations of neurons in the prefrontal cortex of the macaque monkey. J Neurosci 13:2982–2992.

Wang QX, Tanigawa H, Fujita I. 1998. Postnatal development of horizontal axons in the inferior temporal and primary visual cortices in the monkey. Soc Neurosci Abstr 24:900.

Wong-Riley M. 1979. Changes in the visual system of monocularly sutured or enucleated cats demonstrable with cytochrome oxidase histochemistry. Brain Res 171:11–28.

Wong-Riley MT, Carroll EW. 1984. Quantitative light and electron microscopic analysis of cytochrome oxidase-rich zones in VII prestriate cortex of the squirrel monkey. J Comp Neurol 222:18–37.

Xu LH, Tanigawa H, Fujita I. 1997. Modular structure and cortical hierarchy displayed by distribution of AMPA-type glutamate receptors in the monkey ventral visual cortical pathway. Soc Neurosci Abstr 23: 2062.

Yoshioka T, Levitt JB, Lund JS. 1992. Intrinsic lattice connections of macaque monkey visual cortical area V4. J Neurosci 12:2785–2802.

Yukie M, Iwai E. 1988. Direct projections from the ventral TE area of the inferotemporal cortex to hippocampal field CA1 in the monkey. Neurosci lett 88:6–10.

Zeki S, Shipp S. 1988. The functional logic of cortical connections. Nature 335:311–317.